Structure and electrochemical properties of Zn and Co dual-doped ($Li_2Co_{1-x}Zn_xMn_3O_8$) as cathode material for rechargeable lithium-ion batteries

Tze Qing Tan[1, 2], *Rozana Aina Maulat* Osman[1, 3], M. V. Reddy[4], *Shing Fhan* Khor[5] and *Mohd Sobri* Idris[1, 2*]

[1] Centre for Frontier Materials Research, Universiti Malaysia Perlis, 01000 Kangar, Perlis, Malaysia.
[2] School of Materials Engineering, Universiti Malaysia Perlis, Jejawi, 02600 Arau, Perlis, Malaysia.
[3] School of Microelectronics Engineering, Universiti Malaysia Perlis, Pauh Putra, 02600 Arau, Perlis, Malaysia.
[4] Advanced Batteries Lab, Department of Physics, National University of Singapore, Singapore 117542, Singapore.
[5] School of Electrical System Engineering, Universiti Malaysia Perlis, Pauh Putra, 02600 Arau, Perlis, Malaysia.

Abstract. Spinel Zn doped $Li_2CoMn_3O_8$ (or also known as $LiCo_{0.5}Mn_{1.5}O_4$) yielding formula $Li_2Co_{1-x}Zn_xMn_3O_8$ ($0 \leq x \leq 1$) were produced via conventional solid state method. XRD results and the variation of cell lattice and volume showed that the solid solution limit of these compositions was at x=0.6. Impurities were detected when the amount of Zn was beyond 60 %. The discharge capacities deteriorate as Zn content was increased. However, these Zn doped samples exhibited excellent cycle-ability (99.9% capacity retention) throughout 50 charging and discharging cycles which indicated that doping of Zn could possibly stabilised the spinel structure.

1 Introduction

The significant finding of the first Li-ion cells by Sony in the early 1990s has strongly motivated the researches for better performance active materials in order to provide energy storage for some major applications, such as portable electronic devices and other potential applications. Considering cathode materials contributed the most influence on the performance of current Li-ion batteries, a wide variety of studies on cathode materials have been done for the past few decades to fully understand the factors that influence the electrochemical performance of lithium ion batteries and at the same time reducing the cost and simplifying the fabrication process.

An alternative spinel $LiMn_2O_4$ based cathode materials have been proposed as one of the most anticipating cathode materials after the discovery of lithium intercalation-deintercalation reversibility in $LiMn_2O_4$ by Thackeray and co-workers [1]. In addition, it is low cost, thermally stable and benevolent to the environment. Spinel $LiMn_2O_4$ with space group Fd-3m comprises lithium ions on tetrahedral 8a sites and manganese ions on octahedral 16d sites while oxygen ions in 32e sites [2]. However, this spinel suffered from capacity fading which becomes a huge hindrance from feasible use as cathode materials. The capacity fading especially at elevated temperature was due to the existence of cooperative Jahn-Teller distortion when more than 50% of Mn^{3+} appeared [3]. One of the many solutions to reduce this fading is by replacing Mn partially by other elements (M) to increase the Mn valence in the spinel phase, and hence reducing the possibility of the presence of Jahn-Teller distortion. Such doping includes Ru [4], Gd [5], Cu [6], Co [7], Al [8], Mg [9,10], Zn [11], Ni [12] and others. Recently, there are studies focusing on dual substitutions to improve the structural stability and consequently its electrochemical performance [13–15]. On the basis of available literatures, it can be deduced that an interesting composition $LiM_{0.5}Mn_{1.5}O_4$ where exactly ¼ of the Mn was substituted can favour an ordering of 16d cations. Moreover, it is reported previously that substitution of Zn in $LiM_{0.5}Mn_{1.5}O_4$ resulted in a superstructure primitive cubic symmetry [11]. In addition, there are reports about Li-Zn cation inversion where partial Zn ions were located at Li ions sites [16,17].

Hence, in this study, we prepared $Li_2Co_{1-x}Zn_xMn_3O_8$ by conventional solid-state reaction and characterized its structure as a function of Zn content. Structure and morphology of the compounds were characterised by X-ray diffraction (XRD) and scanning electron microscopy (SEM). Furthermore, this study also reports the electrochemical performance of Zn doped $Li_2CoMn_3O_8$.

2 Experimental

Zn doped $Li_2CoMn_3O_8$ ($Li_2Co_{1-x}Zn_xMn_3O_8$) was produced via conventional solid state method [18] using acetate salts as starting materials. Stoichiometric amounts of lithium, cobalt, manganese, and zinc acetates were mixed and ground in acetone to aid homogenous mixing and grounding. Then, the compounds were heated at 400 °C for 12 hours with slow heating rate to

* Corresponding author: sobri@unimap.edu.my

remove acetates. After that, the compounds were heated at 800 °C for 12 hours in air. A Bruker D2 Phaser benchtop X-ray diffractometer equipped with LYNXEYE 1D-detector with Cu-K_α radiation was used. The diffraction patterns were recorded using step size of 0.02˚ and exposure time 1 second per step. Least-square refinements of XRD data were performed using GSAS/EXPGUI [19,20] software to determine the structural parameters.

Electrochemical characterisation of all the synthesised compounds were performed by using a 2016 coin cell (20 mm outside diameter and 1.6 mm thickness). The cell was composed of synthesised compound as a cathode and a metallic lithium as an anode separated by a Celgard 2502 membrane separator with a solution of 1M $LiPF_6$ in ethylene carbonate (EC) + dimethyl carbonate (DMC) + diethyl carbonate (DEC) (with mixing ratio of 1:1:1 Vol. %) as the electrolyte. The cathodes were prepared by mixing active material ($Li_2Co_{0.5}Zn_{0.5}Mn_3O_8$), super P carbon black and the binder poly(vinylidene fluoride) (PVdF: Kynar 2801) in weight percent ratio of 70:15:15 with small amount of N-methyl pyrrolidone (NMP) to form slurry. Then, the obtained slurry was coated on aluminium foil current collector and dried at 80 °C overnight. Then, the prepared electrode was kept in a vacuum oven for 24 h at 70 °C before being used in the Ar-filled glove box (MBraun, Germany) which was maintained at O_2 and H_2O level of less than 2 ppm. The cells were aged for at least 8 h before measurement. Galvanostatic charge-discharge cycling was carried out at room temperature by using a computer-controlled Bitrode multiple battery testers (Model SCN, Bitrode, USA) at a constant current density of 15 mA g^{-1} (C/10).

3 Results and discussion

Fig. 1 shows the XRD patterns of $Li_2Co_{1-x}Zn_xMn_3O_8$ ($0 \le x \le 1.0$) that were prepared at 800 °C in air. For the parent composition $Li_2CoMn_3O_8$ (x=0), the XRD pattern was matched with the ICDD database (No. PDF card: 01-070-4214). Furthermore, its reflections could be indexed by the cubic spinel structure with the space group of Fd-3m. For the Zn-doped $Li_2CoMn_3O_8$, the XRD patterns for $Li_2Co_{1-x}Zn_xMn_3O_8$ ($0 \le x \le 0.4$) were reasonably similar, except a small shoulder at the (400) reflection getting stronger as the amount of Zn was increased. However, the XRD patterns for x=0.6, 0.8 and 1.0 exhibited numerous additional reflections that could be indexed by the primitive symmetry with the space group of $P2_13$. But three reflections were unable to be indexed (denoted as *) and it was believed that they belong to $ZnMn_3O_8$.

In this case, it is speculated that for $x \ge 0.2$, the presence of relatively higher intensity of 220 reflection (2θ= ~31°) compared to the parent $Li_2CoMn_3O_8$ was probably due to Li-Zn cation inversion occurred whereby a partial of Zn ions are located at tetrahedral 8 (a) sites instead of octahedral 16 (d) sites as proposed by Ohzuku *et al*. [16] This occurrence of Li-Zn cation inversion is plausibly because of the strong tetrahedral preference of Zn^{2+}. This partial occupancy of immobile Zn ions in the Li site will probably obstruct the diffusion of Li ions.

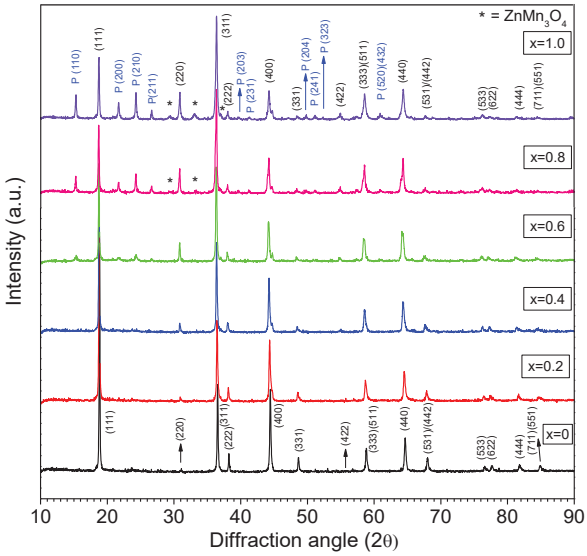

Fig. 1. XRD patterns of $Li_2Co_{1-x}Zn_xMn_3O_8$ compounds that were synthesised at 800 °C.

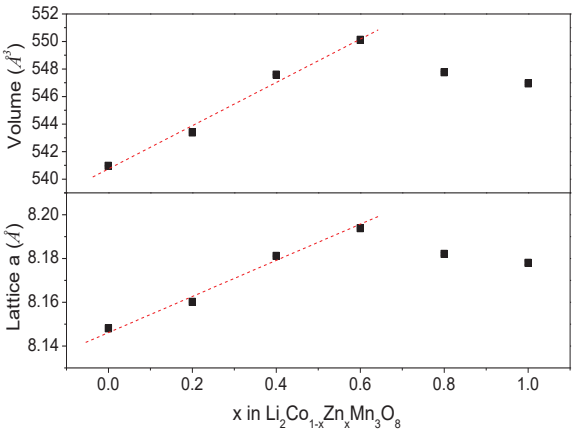

Fig. 2. Variations of structural parameters *a* and unit cell volume as a function of Zn content.

The variations of structural parameters and unit cell volume obtained by the least-square refinements of XRD data were shown in Table 1 and Fig. 2. The structural parameter and unit cell volume of the parent composition $Li_2CoMn_3O_8$ (x=0) obtained from least-square refinements were a=8.1481(1) Å and V=540.96(1) $Å^3$, respectively. The structural parameters and unit cell volume increased linearly within the error (3 e.s.d.s) until x=0.6, followed by slight reduced for x=0.8 and above. The changes of structural parameters obeyed the Vegard's law as the impurities were observed in the XRD patterns for x=0.8 and 1.0. Thus, the solid solution limit for the $Li_2Co_{1-x}Zn_xMn_3O_8$ was x=0.6.

The increase of structural parameters is probably due to the octahedral substitution of Zn^{2+} ions (0.74 Å) which have larger ionic radii compared to Co^{3+} (0.545 Å) ions [21]. However, the structural parameters decreased beyond x=0.6 was possibly due to the increase of Li/Zn cation inversion as mentioned previously whereby the ionic radii of Zn^{2+} ions at tetrahedral sites is 0.60 Å which is smaller than Zn^{2+} at octahedral sites.

Table 1: Structural parameters, unit cell volume and crystallite size of $Li_2Co_{1-x}Zn_xMn_3O_8$ ($0 \leq x \leq 1.0$).

x in $Li_2Co_xZn_{1-x}Mn_3O_8$	Space group	Lattice parameter, a (Å)	Unit cell volume (Å^3)	Crystallite size (Å)
x = 0.0	Fd-3m	8.1481(1)	540.96(1)	661.3
x = 0.2	Fd-3m	8.1602(1)	543.39(1)	604.7
x = 0.4	Fd-3m	8.1812(1)	547.59(1)	594.1
x = 0.6	P2$_1$3	8.1938(1)	550.12(2)	597.9
x = 0.8	P2$_1$3	8.1821(2)	547.76(2)	510.8
x = 1.0	P2$_1$3	8.1780(3)	546.95(3)	493.7

The average crystallite sizes of $Li_2Co_{1-x}Zn_xMn_3O_8$ were calculated by Dybye-Scherrer equation from the line width of the strongest reflection plane which refers to the (311) plane. The average crystallite size for all the samples obtained from the calculations are listed in Table 1. The parent composition $Li_2CoMn_3O_8$ (x=0) exhibited the largest crystallite size (661.3 Å) and the size decreased as Zn content increased whereby x=1 possessed the smallest size of 493.7 Å.

Microstructural images observed by SEM analysis of spinel $Li_2Co_{1-x}Zn_xMn_3O_8$ ($0 \leq x \leq 1$) compounds synthesised at 800 °C are shown in Fig. 3. The images show typical solid state samples with random particle size distribution. Obviously, all the samples exhibit well developed particles of regular shape. The micrographs were taken at an appropriate magnification to emphasize the morphology of the samples. It is noticeable that all the particles are in micron size (< 5 µm). From observation, the primary particle size increases as the Zn content increases.

Fig. 4 depicted the galvanostatic charge-discharge profile for 1st, 2nd, and 50th cycle of $Li_2Co_{1-x}Zn_xMn_3O_8$ compounds that were synthesised at 800 °C. The cycling tests were carried out at a current rate of 15 mA g^{-1} in the voltage window of 2.5-4.6 V vs. Li. All the cells possessed ~ 3.0 V of open circuit voltage and a flat voltage profile at ~4.0 V where the oxidation and reduction reaction occurs (except for x=0.8 and 1.0).

The discharge capacities vs cycle number plots were shown in Fig. 5. The discharging capacities deteriorated as doping of Zn increased. The initial discharging capacity of undoped $Li_2CoMn_3O_8$ is ~115.7 mAh g^{-1} which was comparable to the theoretical capacity value (~147 mAh g^{-1}). The discharge capacity faded about 11.11 % after 50 cycles. Furthermore, the initial discharging capacity decreased from ~115.7 mAh g^{-1} to ~ 68.1 mAh g^{-1}, ~ 63.7 mAh g^{-1} and ~48.4 mAh g^{-1} when 20 %, 40 % and 60 % of Co was replaced by Zn, respectively. The discharging capacity dropped to ~15.6 mAh g^{-1} and ~7.7 mAh g^{-1} when 80 % and 100 % of Zn was doped. Although the discharging capacities continue to decrease as more Co was replaced by Zn, but the discharge capacities can be retained approximately 99.9 % after 50 cycles for all the Zn doped samples. It is speculated that the capacities were affected by the immobile Zn ions in the Li site which obstructed the diffusion of Li ions. Nonetheless, the doping of Zn stabilized the structure during charging and discharging cycle.

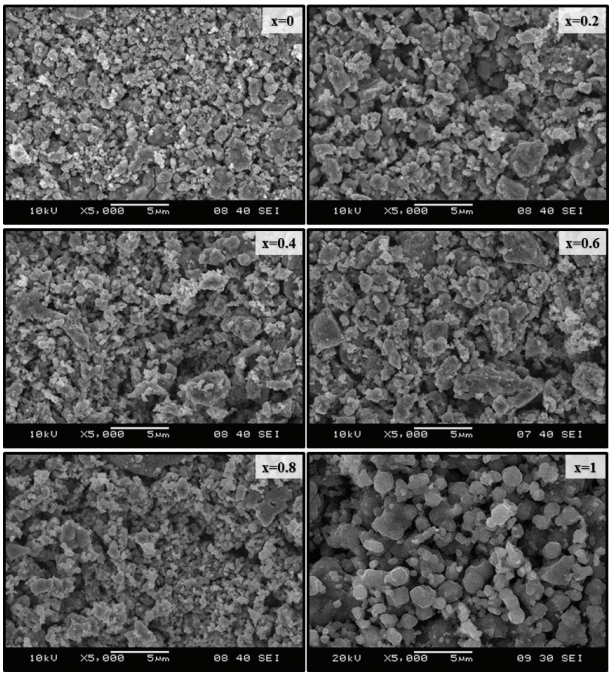

Fig. 3. SEM images of $Li_2Co_{1-x}Zn_xMn_3O_8$ ($0 \leq x \leq 1$) compounds at magnification of 5000×.

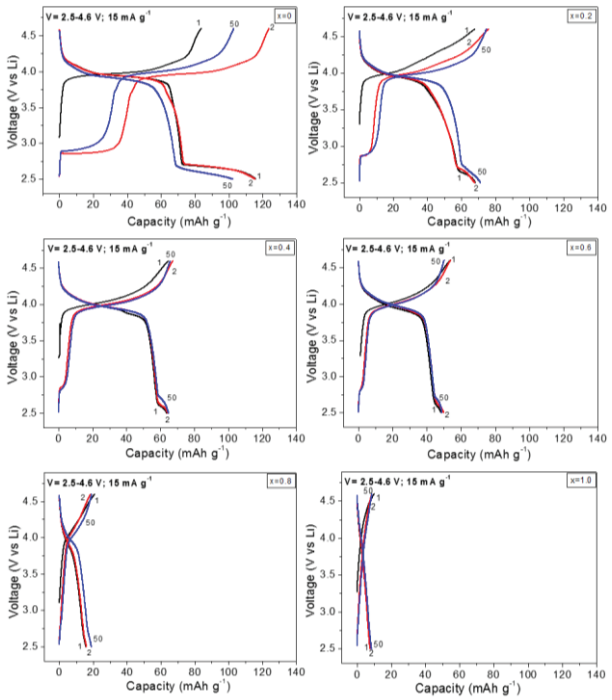

Fig. 4. The galvanostatic charge-discharge profile for 1st, 2nd, and 50th cycle of $Li_2Co_{1-x}Zn_xMn_3O_8$ ($0 \leq x \leq 1$) compounds that were synthesised at 800 °C.

* Corresponding author: sobri@unimap.edu.my

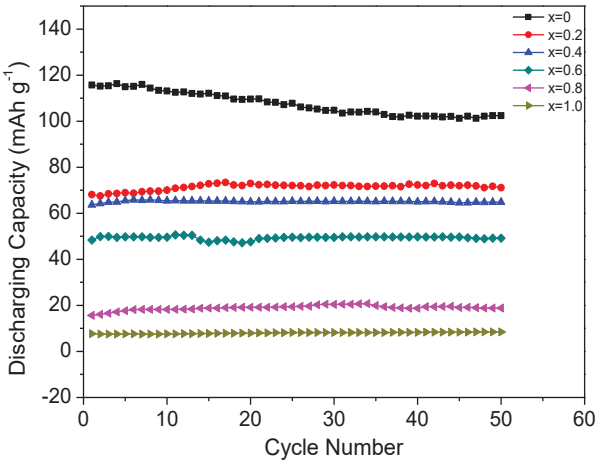

Fig. 5. The discharge capacities vs cycle number plots of $Li_2Co_{1-x}Zn_xMn_3O_8$ ($0 \leq x \leq 1$) compounds that were synthesised at 800 °C.

4 Conclusion

Zn doped $Li_2CoMn_3O_8$ ($Li_2Co_{1-x}Zn_xMn_3O_8$) were synthesised via simple conventional solid state route. In this systematic study, the relationship of the Zn content and electrochemical performance of Zn doped $Li_2CoMn_3O_8$ ($Li_2Co_{1-x}Zn_xMn_3O_8$) was established. Li/Zn cation inversion is believed to impede the diffusion of Li ion and hence influenced the discharge capacity. However, Zn was found to stabilise the spinel structure as these Zn-doped compositions demonstrated a stable cycle-ability in Li-ion batteries. Further investigation will be done to determine or estimate the amount of Li-Zn cation inversion.

The authors would like to acknowledge the Ministry of Higher Education Malaysia for the financial support through the Fundamental Research Grant Scheme 2014 (FRGS Grant No.: 9003-00429). We acknowledged the support of the National University of Singapore in providing the Advanced Batteries Research facilities used in this work.

References

1. M. M. Thackeray, W. I. F. David, P. G. Bruce, and J. B. Goodenough, Mater. Res. Bull. **18**, 461 (1983).
2. J. M. Tarascon, J. Electrochem. Soc. **138**, 2859 (1991).
3. G. Amatucci, A. Du Pasquier, A. Blyr, T. Zheng, and J.-M. Tarascon, Electrochim. Acta **45**, 255 (1999).
4. M. V Reddy, S. S. Manoharan, J. John, B. Singh, G. V. Subba Rao, and B. V. R. Chowdari, J. Electrochem. Soc. **156**, A652 (2009).
5. S. C. Han, S. P. Singh, Y. -h. Hwang, E. G. Bae, B. K. Park, K.-S. Sohn, and M. Pyo, J. Electrochem. Soc. **159**, A1867 (2012).
6. H.-W. Chan, J.-G. Duh, and H.-S. Sheu, J. Electrochem. Soc. **153**, A1533 (2006).
7. C. H. Shen, R. S. Liu, R. Gundakaram, J. M. Chen, S. M. Huang, J. S. Chen, and C. M. Wang, J. Power Sources **102**, 21 (2001).
8. L. Xiao, Y. Zhao, Y. Yang, Y. Cao, X. Ai, and H. Yang, Electrochim. Acta **54**, 545 (2008).
9. B. Deng, H. Nakamura, Q. Zhang, M. Yoshio, and Y. Xia, Electrochim. Acta **49**, 1823 (2004).
10. G.-M. Song, W.-J. Li, and Y. Zhou, Mater. Chem. Phys. **87**, 162 (2004).
11. Y. J. Lee, S.-H. Park, C. Eng, J. B. Parise, and C. P. Grey, Chem. Mater. **14**, 194 (2002).
12. C. A. Kim, H. J. Choi, J. H. Lee, S. Y. Yoo, J. W. Kim, J. H. Shim, and B. Kang, Electrochim. Acta **184**, 134 (2015).
13. D.-L. Fang, J.-C. Li, X. Liu, P.-F. Huang, T.-R. Xu, M.-C. Qian, and C.-H. Zheng, J. Alloys Compd. **640**, 82 (2015).
14. R. Thirunakaran, R. Ravikumar, S. Gopukumar, and A. Sivashanmugam, J. Alloys Compd. **556**, 266 (2013).
15. H. Zhang, Y. Xu, D. Liu, X. Zhang, and C. Zhao, Electrochim. Acta **125**, 225 (2014).
16. T. Ohzuku, S. Takeda, and M. Iwanaga, J. Power Sources **81**–**82**, 90 (1999).
17. P. Strobel, A. Ibarra-Palos, M. Anne, C. Poinsignon, and A. Crisci, Solid State Sci. **5**, 1009 (2003).
18. T. Q. Tan, M. S. Idris, R. A. M. Osman, M. V. Reddy, and B. V. R. Chowdari, Solid State Ionics **278**, 43 (2015).
19. A. C. Larson and R. B. Von Dreele, Los Alamos Natl. Lab. Rep. LAUR **748**, 86 (2004).
20. B. H. Toby, J. Appl. Crystallogr. **34**, 210 (2001).
21. R. D. Shannon, Acta Crystallogr. Sect. A **32**, 751 (1976).